El Niño/Southern Oscillation Predictability

KLAUS FRAEDRICH

Bureau of Meteorology Research Centre, Melbourne, Australia

(Manuscript received 18 March 1987, in final form 28 October 1987)

ABSTRACT

Predictability time scales are estimated from annual time series of the El Niño/Southern Oscillation (ENSO). They are defined by the rate of divergence of initially close independent pieces of trajectories in phase space. Fitted stochastic processes and the nonlinear deterministic analysis of the empirical time series lead to *e*-folding predictability time scales up to 1.5 years (or one year of error doubling time) indicating that at least a skillful nowcasting of ENSO may be possible. Due to sparse data these estimates provide only weak bounds.

1. Introduction

The occurrence of El Niño/Southern Oscillation (ENSO) episodes is highly irregular with time intervals between one and seven years. Therefore, it is not surprising that a similarity with a special class of simple dynamical systems has been suggested, which are deterministic and show chaotic behavior with sensitive dependence on initial conditions. Accordingly, the time evolution in phase space is assumed to evolve on a strange attractor of relatively low dimensionality (e.g., Vallis 1986; Fraedrich 1987b); related limits of predictability depend on the growth rate of amplifying instabilities separating initially close states. This represents the purely dynamical approach towards predicting ENSO. For example, Cane et al. (1986) claim from their numerical modeling results (of a coupled tropical ocean–atmosphere system) "that El Niño is generally predictable one or two years ahead." On the other side of the spectrum of ENSO prediction schemes lie the purely statistical forecasting techniques (e.g., based on parsimonious multivariate time lagged regressions), from which "sea surface temperature (SST) anomalies during 1982–83 in the equatorial Pacific could have been predicted 4–5 months in advance" (Barnett 1984). But whether these prediction time scales coincide with limits of ENSO predictability remains open. Estimates on the natural ENSO predictability, however, should be available when setting up strategies for ENSO prediction model building.

One way towards ENSO prediction is to forecast the time evolution of its spatial patterns once the first signs of an event start to appear (which is in the early months of a calendar year). For example, in major ENSO events, the sequence of associated oceanic and atmospheric anomalies evolve similarly in time. Equatorial Pacific sea surface temperature anomalies increasing early in the calendar year, peak in December/January and vanish about April. Atmospheric anomaly fields show similar phase, locking to the annual cycle.

The other way is to predict the occurrence of an ENSO event before any obvious signals appear; this will be discussed in the following. Therefore, any strong influence of the annual cycle needs to be eliminated, because it apears to dominate monthly ENSO time signals (rainfall, pressure, sea surface temperatures) when subjected to a nonlinear analysis. Thus ENSO time series are analyzed based on appropriate annual means from April to March.

In section 2 the definition of predictability and its meteorological and physical background are outlined, as are the methods of how to estimate it from a single variable time series. In section 3 the methodology is applied to a hierarchy of stochastic models of discrete and continuous states (fitted to the ENSO time series) to provide a suitable standard of comparison for the nonlinear deterministic analysis of the annual ENSO signal (section 4). Conclusions discuss the limitations of the analysis.

2. Estimating ENSO predictability: Basic concepts and data

Predictability of a dynamical system like ENSO is closely related to the problem of its stability during the time evolution. For example, consider the difference between two states of a deterministic process. If this difference is small initially and remains small in the future, the process is stable and predictable. Conversely, if the initially small difference exceeds a threshold value the process is unstable and eventually becomes unpredictable. Thus, a relevant measure of predictability of

Corresponding author address: Prof. K. Fraedrich, on leave from Freie Universitat Berlin, Institut für Meteorologie, D-1000 Berlin 41, West Germany.

a system is the rate at which initially small errors grow. To measure the predictability two routes are followed (Lorenz 1984).

a. Basic concepts

In the traditional approach to estimate the predictability of a dynamical system one evaluates the distance between two initially only slightly different states by solving the nonlinear equations twice with different sets of initial conditions:

$$\frac{dx_i}{dt} = f_i(x_i, \cdots, x_n). \tag{2.1}$$

The x_i are n suitably normalized variables spanning the n-dimensional phase space.

Alternatively, error growth rates in a dynamical system can also be determined by the set of i (= $1, \cdots, n$) linear differential equations of small deviations, δx. The coefficients $A(i, j) = \partial f_i/\partial x_j$ at $x(t)$ are elements of the Jacobian matrix of (2.1) and vary with the time evolution (Lorenz 1965):

$$\frac{d\delta x_i}{dt} = \sum_{j=1}^{n} A(i, j)\delta x_j. \tag{2.2}$$

The eigenvectors of $A(i, j)$ provide a local coordinate system, which describes the semi-axes of an infinitesimally small error sphere expanding into an ellipsoid. After suitable time averaging the associated positive characteristic exponents (i.e., Lyapunov exponents), $\lambda_i(x_0, \delta x_0) > 0$, can be used to define the predictability (for details see Lorenz 1985, and also e.g. Ghil and Childress 1987) as the average rate of divergence of an infinitesimally small phase space volume (i.e., only the diverging axes, $\lambda_i > 0$, contribute):

$$K = \sum_{\lambda_i > 0} \lambda_i. \tag{2.3}$$

Applying this approach to observations, one should note that (for smooth continuous evolution, Pesin 1977) this average growth rate (2.3) is equivalent to the average production of information per unit time (Kolmogoroff entropy). As the information production can also be defined in probabilistic terms, it can, at least in principle, be estimated from data. For practical purposes the order-2 entropy K_2 suffices as an estimator (see Grassberger and Procaccia 1983, 1984 for more details):

$$K > K_2$$

$$= -\lim \frac{1}{m\tau} \ln\Big[\sum_{i_0 \cdots i_{m-1}} p^2(i_0, \cdots, i_{m-1})\Big] \tag{2.4}$$

for $m \to \infty$, $\tau \to 0$; the sum $\sum p^2(i_0, \ldots, i_{m-1})$ is the probability that a pair of pieces of time trajectories in the state space (of dimension n), $x(t_i)$, $x(t_j)$, falls into the same sequence of boxies $(i_0, \ldots, i_{m-1})$ of the space-time (l, τ) partitioning with $(l, \tau) \to 0$, while the system evolves from t_i, t_j to $t_i + (m-1)\tau$, $t_j + (m-1)\tau$. This is equivalent to the probability that two independent pieces of trajectories of length or duration m remain less than a distance l apart.

When analyzing observations one is generally confined to a single observable, $x(t)$. Therefore suitable substitute phase spaces need to be found. A substitute phase space can be spanned by a sufficiently large number of (say m) time-lag coordinates $x_m(t_i) = [x(t_i), x(t_i + \tau), \cdots, x(t_i + (m-1)\tau)]$ of this single observable (Packard et al. 1980; Takens 1981). For smooth (but not fractal) dynamics it has been shown that in this new phase space the basic geometrical properties of the system are retained: the dimension (say D_2) of the attractor (i.e., a subset of the phase space on which the dynamics of the system evolves after the transients have decayed) and the divergence (say K_2) of nearby pieces of trajectories on it (e.g., see Eckmann and Ruelle 1985). Provided the dimension of this new substitute phase space is sufficiently large to embed the attractor, the predictability of the system may be estimated from a pointwise cumulative number distribution $C_m(l)$ of all pairs of independent pieces of the time series which are less than a distance l apart from one another (Grassberger and Procaccia 1983, 1984):

$$C_m(l) = \frac{1}{N} \sum \Theta(l - r_{ij}(m)) \quad \text{for} \quad N \to \infty, \quad l \to 0 \tag{2.5a}$$

where Θ is the Heavyside-function with $\Theta(a) = 0$ or 1 if $a>$ or <0. The total number of points N (or pieces of the time series) and the distance between two of them is given by the Euclidean norm,

$$r_{ij}(m) = |x_m(t_i) - x_m(t_j)| \tag{2.5b}$$

t_i and t_j denote the beginnings of different (i.e. independent) pieces of the time series. Note that $|t_i - t_j|$ larger than the autocorrelation time of the time series $x(t)$ guarantees the trajectory pieces to be independent. The choice of the time lag τ as the autocorrelation time leads to linearly independent coordinates spanning the substitute (embedding) phase space. This number distribution function $C_m(l)$ estimates an ensemble average over all points (in the substitute phase space of time lagged coordinates) which are less than the distance $r_{ij} < l$ apart. Thus $C_m(l)$ describes the mean relative number of pairs of points found in a phase space volume element (or ball) of radius l; every individual point represents a piece of the time trajectory. With increasing distance threshold l (or size of the ball) the number of pairs of points grows. Furthermore, $C_m(l)$ changes when increasing the duration or length of the trajectory pieces (i.e. when increasing the embedding dimension m). For a sufficiently large number N of points in phase space the distribution function $C_m(l)$ allows to estimate the dimension of an attractor (D_2) and the divergence (K_2) of nearby pieces of trajectories evolving on it

(Grassberger and Procaccia 1983; for applications to observed weather and climate variables see Fraedrich 1986, 1987a; Nicolis and Nicolis 1984); i.e. $C_m(l)$ scales for $m \to \infty$, $l \to 0$ as

$$C_m(l) \sim l^{D_2} \exp(-m\tau K_2). \quad (2.6a)$$

Estimates of the cumulative distribution function are presented in a $\ln C_m(l)$ versus $\ln l$ diagram for increasing embedding dimensions m, i.e. for pieces of trajectories lasting one, two, . . . , m years. From these diagrams one can now evaluate, at least in principle, the dimension of attractors, D_2, and the predictability, $1/K_2$:

$$D_2 \sim \frac{\ln C(l)}{\ln l}, \quad K_2 \sim \frac{1}{\tau} \ln C_m/C_{m+1}. \quad (2.6b)$$

b. El Niño/Southern Oscillation time series

In the following sections, the alternative method of estimating predictability is applied to two ENSO time series, which reliably cover a period of hundred years or more. The time series of annual El Niño intensities (Quinn et al. 1978, updated by Rasmusson 1984) may be related to the oceanographic aspects of the process; it consists of the five discrete categories of no, very weak, weak, moderate, and strong events to which the numbers zero to four are attached. The annual Southern Oscillation index, SOI, is deduced from station pressure anomalies and defined by a continuous variable signal; it appears to characterize the meteorological side of the phenomenon (Wright 1975, and updated, personal communication). Note, however, that the El Niño/Southern Oscillation is a global phenomenon of short term climate fluctuations and its temporal signal can be identified in various meteorological and oceanographic fields. Wright (1984) analyzed a number of such signals (indices) taken from the core regions of both meteorological and oceanographic fields and found that they are almost equivalent on an annual (April to March) basis.

The predictability analysis of the ENSO time series consists of two steps. First, a hierarchy of discrete and continuous state stochastic processes is fitted to the datasets and the predictability of these models is evaluated (section 3), applying the concept described above. Besides demonstrating the methodology, the analysis of stochastic processes provides the appropriate standards of comparison for the nonlinear deterministic analysis of both the discrete and continuous state time series, which comprises the second step and is presented in section 4.

3. Stochastic models of El Niño and the Southern Oscillation

Two classes of stochastic models can be distinguished. They are either discrete or continuous state models depending on the processes to be analyzed.

The hierarchy of discrete state models evolves from a binary process (a biased coin toss) which, in the context of ENSO, can be related to the idea that two complementary states, El Niño and La Niña, describe the El Niño/Southern Oscillation phenomenon (Philander 1985): "During El Niño years the area of high sea surface temperature increases, while the atmospheric convection zones of the tropical Pacific expand and merge so that there is a tendency toward spatially homogeneous conditions. La Niña is associated with low surface temperatures near the equator, with atmospheric convergence zones that are isolated from each other, and with spatial scales smaller than those of El Niño." Quinn et al.'s (1978) annual El Niño intensities provide the data to calibrate such a binary process; La Niña is defined by the zero intensity while the other state, El Niño, is associated with either one of the remaining intensity values. This binary state (coin tossing) system is extended in two directions: k discrete states are introduced to distinguish more intensity levels and a memory is included after estimating the Markov properties of the process.

The class of discrete state stochastic processes needs to be complemented by a hierarchy of continuous state models, because the Southern Oscillation is a continuous phenomenon. It ranges from years (April to March) of major ENSO events through years with small anomalies to years of major anomalies of opposite sign (anti-ENSO). Thus, Gaussian processes of increasing order (or memory) are introduced and fitted to the continuous Southern Oscillation index (Wright 1975; for more details on various Southern Oscillation signals see Wright 1985).

Stochastic processes provide the appropriate standards of comparison for the performance of deterministic forecast models. Analogously, the predictability analyses of the fitted stochastic processes provide the standard of reference for the nonlinear deterministic analysis of the El Niño intensities and the Southern Oscillation index (section 4).

a. El Niño and La Niña as a binary process

Consider the El Niño/Southern Oscillation as a single variable binary (two state) time series, $x(t)$, of an annual time step (or sampling time $\tau = 1$ year). It consists only of El Niño ($x = 1$) and La Niña ($x = 0$) events discarding intensities. If they are taken from Quinn et al. (1978, updated by Rasmusson 1984) using 140 years from 1844–1983, the following probabilities can be attached:

$$\text{prob}\{x(t) = 1 \text{ or El Niño}\} = p_1 \sim 0.41$$

$$\text{prob}\{x(t) = 0 \text{ or La Niña}\} = p_0 = 1 - p_1 \sim 0.59. \quad (3.1)$$

They are defined by the mean (or climate) of the binary time series: $p_1 = 1 - p_0 = \langle x(t) \rangle \sim 0.41$. Its variance $B_c = \langle (x - p_1)^2 \rangle = p_1 - p_1^2 = p_1 p_0 \sim 0.24$ is identical

with the half-Brier score of a probabilistic forecast of El Niño based only on climatology prediction (i.e. using $p_1 = 1 - p_0$ for each year).

A sequence of m successive binary events defines a piece of the single variable time series commencing at $t = t_i$ and proceeding $(m - 1)$ time steps of length τ:

$$x_m(t_i) = [x(t_i), x(t_i + \tau), \cdots, x(t_i + (m-1)\tau)]. \tag{3.2}$$

Such a piece of trajectory represents a state or a point, $x_m(t_i)$ in the m-dimensional phase space spanned by time-lagged coordinates. A pair of two such pieces of trajectories, $x_m(t_i)$ and $x_m(t_j)$, which are initially only an infinitesimally small distance $|\delta x_0|$ apart from one another, tend to separate with each time step τ (from m to $m + 1$). Loss of predictability is defined by the exponential (or doubling) rate of the distances between initially close pieces of trajectories (or states in phase space) increasing with time. In physical systems this separation of initially close pieces of trajectories depends on the growth of perturbations amplified by unstable modes. In a stochastic process this is provided by an information source generating numbers or symbols at discrete time steps. Defining the distance by the Euclidean norm one obtains for its square

$$|x_m(t_i) - x_m(t_j)|^2 = \sum_{\gamma=0}^{m-1} [x(t_i + \gamma\tau) - x(t_j + \gamma\tau)]^2. \tag{3.3}$$

For binary time series, $x(t)$, each of the m squared distance components (related to each time lag coordinate) is also a binary variable, i.e. $\Delta x^2(i, j) = (x(t_i + \gamma\tau) - x(t_j + \gamma\tau))^2 = 0$ or 1 for $\gamma = 0, 1, \cdots m - 1$.

Assume the trajectory, $x(t)$, is generated by the same random source (namely a Bernoulli trial with biased coinflips, i.e., El Niño with $p_1 = 0.41$, La Niña with $p_0 = 0.59$). Then every squared distance component, $\Delta x^2(i, j) = 0$ or 1, in (3.3) is also a binary random variable which is independent of the γth coordinate to which it belongs. The associated probabilities of their occurrence result from the conditional probabilities of stochastically independent events which are mutually exclusive (e.g., Feller 1950):

$$\begin{aligned}\text{prob}(\Delta x^2 = 0) &= \text{prob}\{x(t_i + \gamma\tau) = 0 \,|\, x(t_j + \gamma\tau) = 0\} \\ &\quad + \text{prob}\{x(t_i + \gamma\tau) = 1 \,|\, x(t_j + \gamma\tau) = 1\} \\ &= p_0^2 + p_1^2 = q \sim 0.5162\end{aligned}$$

$$\begin{aligned}\text{prob}(\Delta x^2 = 1) &= \text{prob}\{x(t_i + \gamma\tau) = 0 \,|\, x(t_j + \gamma\tau) = 1\} \\ &\quad + \text{prob}\{x(t_i + \gamma\tau) = 1 \,|\, x(t_j + \gamma\tau) = 0\} \\ &= 2p_0p_1 = p \sim 0.4838.\end{aligned} \tag{3.4}$$

Thus, all m elements of the sum (3.3) leading to the squared distance between pairs of trajectories are given by independent binary random numbers of another Bernoulli experiment of biased coinflips for which $p = \langle \Delta x^2 \rangle$ is given by (3.4). Therefore the sum of the m-squared distance components (partial distances) is bionomially distributed:

$$\begin{aligned}\text{prob}\{|x_m(t_i) - x_m(t_j)|^2 = l^2\} &= b(l^2, m, p) \\ &= \binom{m}{l^2} p^{l^2} (1-p)^{m-l^2}\end{aligned} \tag{3.5}$$

where $b(l^2, m, p)$ is the binomial distribution.

The cumulative distance distribution $C_m(l)$ (section 2) describes the probability (or relative frequency) of pairs of independent pieces of trajectories of the same length m, which are less than a distance l apart:

$$\begin{aligned}C_m(l) &= \text{prob}\{|x_m(t_i) - x_m(t_j)| \leqslant l\} \\ &= \sum_{l^2} b(l^2, m, p) \quad \text{for} \quad l^2 = 0, 1, 2, \cdots.\end{aligned} \tag{3.6}$$

The smallest distance possible between two pieces of trajectories is $l = 0$, the largest one is $l = \sqrt{m}$. The probability (or relative number) of independent pairs of pieces of trajectories to remain unseparated ($l = 0$, i.e. identical to each other or a vanishing distance apart) for m successive sampling points (events) can now be deduced from (3.5) or (3.6):

$$C_m\,(l = 0) = C_m(l < 1) = q^m = (p_0^2 + p_1^2)^m. \tag{3.7}$$

Thus, the order-2 entropy can be determined from (2.6) using (3.7) as a measure of information gain per unit time step ($\tau = 1$ year):

$$K_2 = -\frac{1}{\tau} \ln(p_0^2 + p_1^2) \sim 0.66 \text{ per year.} \tag{3.8a}$$

This leads to a predictability time scale, $1/K_2 \sim 1.5$ years, characterizing an e-folding error expansion rate. For doubling multiply with $\ln 2 \sim 0.69$, which yields a time scale of about one year. Note that K_2 is a lower bound of the Kolmogoroff entropy $K = \tau^{-1}(p_0 \ln p_0 + p_1 \ln p_1) \sim 0.68$ per year.

For an unbiased coinflip El Niño, i.e. $p_0 = p_1 = 0.5$, $K = K_2$ with predictability or error doubling time scales of exactly one year. This predictability or error doubling time scale, $1/K_2 = \tau$, is due to the number of only two (and equally probable) discrete states. Increasing the number of equally probable states would decrease the predictability bound to zero. In appendix A the distance distributions of the observed and (random) biased coinflip binary time series are compared.

1) FINITE NUMBER OF STATES

Increasing the number of states with probabilities p_i, where $i \geqslant 2$, leads to a polynomial distribution replacing the binomial one in (3.5) and (3.6). Corre-

spondingly $C_m(l=0) = (\sum_i p_i^2)^m$ in (3.7) and the order-2 entropy yields

$$K_2 = -\frac{1}{\tau} \ln \sum_{i=0}^{k-1} p_i^2. \quad (3.8b)$$

Thus, increasing the number $i = 0, 1, \cdots, k-1$ to k equally probable states, $p_i = 1/k$, would decrease the predictability to $1/K_2 = \tau/\ln k$.

As an example we take the bimodally distributed five state El Niño intensity time series from Quinn et al. (1978, updated by Rasmusson 1984), which has been adopted to model chaotic ENSO dynamics (Fraedrich 1987b). The $k = 5$ intensity states and their climate probabilities (estimated from 1844 to 1983) are no El Niño ($p_0 \sim 0.59$), very weak ($p_1 \sim 0.05$), weak ($p_2 \sim 0.09$), moderate ($p_3 \sim 0.14$), and strong El Niño ($p_4 \sim 0.13$). This leads to a predictability time scale of $1/K_2 \sim 1.08$ years (3.8b) or about 0.75 years error doubling time. Not unexpectedly, this is considerably less than the binary time series estimates (due to their reduced number of states), but—due to bimodality—larger than the predictability time scale of $k = 5$ equally probable states, which yields $1/K_2 = \tau/\ln k \sim 0.62$ years or 0.43 years error doubling time.

2) Markov chain model

The biased coinflip El Niño/La Niña may be used as a reference stochastic prediction scheme against which higher order schemes should be tested. It may be interpreted as a zero-order two-state Markov chain whose transition probabilities, $p_{kl} = \text{prob}\{x(t+\tau) = l | x(t) = k\}$ with $x = 0$ or 1, are identical with the climate probabilities p_0 and p_1. The climate state occupation probabilities for El Niño ($x = 1$) or La Niña ($x = 0$) events are shown in Table 1 leading to the zero-order Markov chain, with a hindcast half-Brier score $B_c \sim 0.24$ (see above):

$$p_{00} = p_{10} = p_0 \sim 0.59 \pm 0.11$$
$$p_{01} = p_{11} = p_1 \sim 0.41 \pm 0.13. \quad (3.9)$$

For more detailed probabilistic predictions the El Niño events may be modeled as a higher (e.g. first order) Markov chain whose transition probabilities from state k to state l form a transition matrix p_{kl}. Forecasts map a stochastic initial state vector a_k to a future probability vector $a_l = a_k p_{kl}$, which tends to the climate state probabilities $a_l \to (p_0, p_1, \ldots)$ after successive mappings. Accordingly the transition matrix p_{kl} tends to the climate state (equilibrium) transition matrix (for $m \to \infty$) with identical column elements defined by the climate state occupation probability $(p_0, p_1, \ldots)$.

With the (e.g. maximum likelihood) estimates of the transition probabilities p_{kl} (Table 1) (a) the Markov property of the time series needs to be tested (to justify the model application) and (b) the order of the Markov process needs to be defined. Thus the transition matrix of climate or zero-order probability predictions is compared with those of successively higher-order models. It appears that the first-order Markov chain is significantly different from the zero-order or equilibrium matrix (and not from the second order one) only on a 90% level; i.e. at a 95% significance level the null hypothesis cannot be rejected that first, zero and second order chains are indistinguishable (see Anderson and Goodman 1957; Lowry and Guthrie 1968). Thus, the first-order Markov process seems to be the highest order which can be fitted to the binary El Niño time series taken from Quinn et al. (1978). Still, there is strong similarity between the outcome of a first- and zero-order process which is also reflected by the observed and fitted distributions of the residence, recurrence, and first passage times of the El Niño/La Niña binary events (Fig. 1, for definitions see appendix B). Furthermore, the first-order Markov hindcast half-Brier score $B_M = \{38(1-p_{01})^2 + 18(1-p_{11})^2 + 42p_{01}^2 + 38p_{11}^2\}/138 \sim 0.23$ deduced from Table 1 shows only a negligibly small improvement over the climate prediction ($B_c \sim 0.24$). Therefore it is not surprising to obtain a predictability time scale for El Niño/La Niña events produced by a (first-order) Markov source (e.g., Farmer 1982), which is of similar magnitude as the climate or unfair coinflip process:

$$K_2 = -\frac{1}{\tau}\{p_0 \ln(p_{00}^2 + p_{01}^2) + p_1 \ln(p_{10}^2 + p_{11}^2)\}. \quad (3.10)$$

Introducing the estimated transition probabilities (Table 1) we obtain an e-folding predictability time scale of $1/K_2 \sim 1.6$ years. The corresponding doubling times are only slightly more than year; the similarity with the magnitude of the sampling time is not surprising due to the weaker Markov and stronger random nature of the binary dataset. Note that Markov chain models have recently received growing attention in both short term weather prediction and large scale dynamics/extended range forecasting (e.g., Mo and Ghil 1987, de Swart and Grasman 1987, etc.).

b. *El Niño/Southern Oscillation as a continuous process*

Now consider the Southern Oscillation measured by a continuous single variable time series, $x(t)$, of annual sampling time ($\tau = 1$ year). As an example we use 100 years (1884–1983) of Wright's (1975, and updated) Southern Oscillation index (SOI) defining a year appropriately from April to March. This index is almost Gaussian distributed with estimated mean ~ 1.5, variance ~ 48.9, skewness ~ 0.38, and kurtosis ~ 3.1; the following frequencies are observed in the eight SOI classes of 5 integer units decreasing from 25 to -14: 1, 2, 10, 15, 27; 28, 10, 7. Thus, a suitable stochastic representation of this continuous annual time series appears to be the (stationary) Gaussian process. In

RESIDENCE TIME
EL NINO

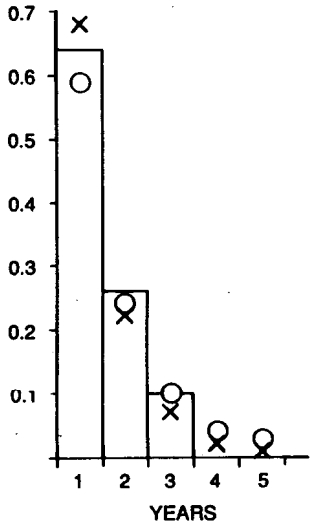

RESIDENCE TIME
LA NINA

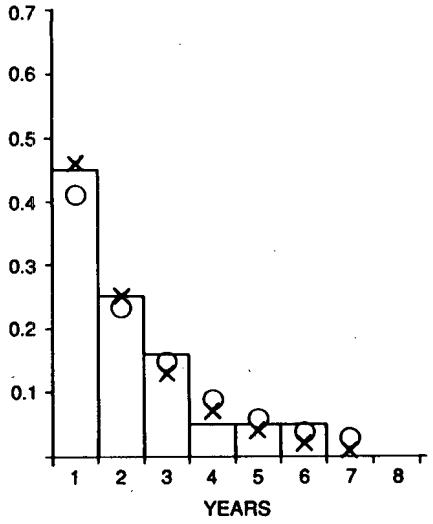

RECURRENCE TIME
LA NINA – LA NINA

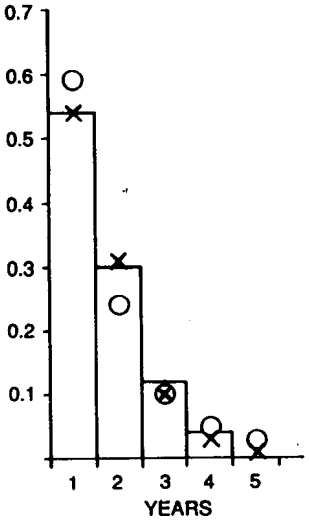

RECURRENCE TIME
EL NINO – EL NINO

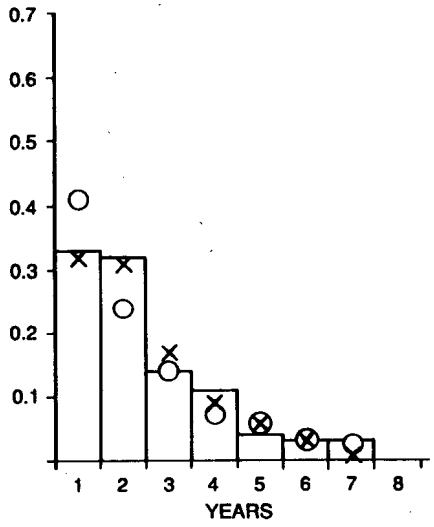

FIRST PASSAGE TIME
EL NINO – LA NINA

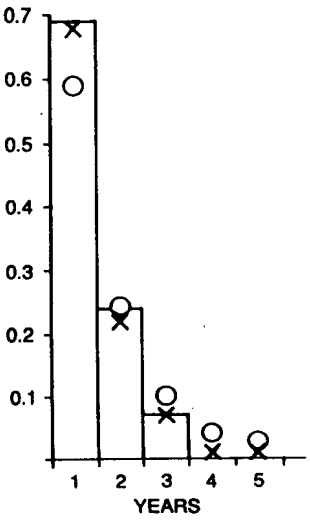

FIRST PASSAGE TIME
LA NINA – EL NINO

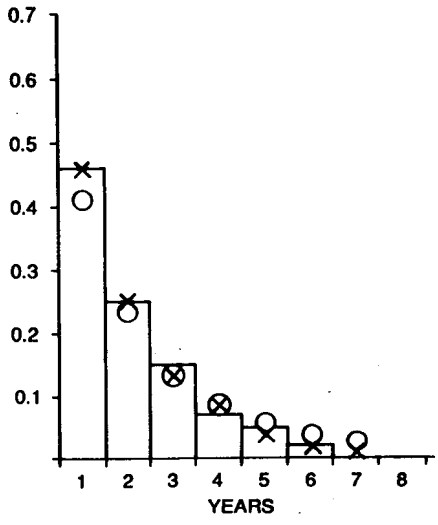

TABLE 1. Estimated conditional frequencies and transition probabilities (±95% confidence limits) for present (t) and preceding ($t-1$) El Niño/La Niña states; bottom: equilibrium (climate) state occupation probabilities.

	t				
$t-1$	La Niña	El Niño	Σ	La Niña	El Niño
La Niña	44	38	82	.54 ± .15	.46 ± .16
El Niño	38	18	56	.68 ± .15	.32 ± .22
Climate	82	56	138	.59 ± .11	.41 ± .13

analogy to the binary time series (§3a; produced by a zero- and first-order Markov source), we analyze a zero- and first-order autoregressive (AR) process (e.g., Cox and Miller 1965), which is normalized to zero mean ($x = 0$) and unit variance $\sigma_x^2 = 1$:

$$x(t_i) = \lambda x(t_{i-1}) + z(i) = \sum_{n=0}^{\infty} \lambda^n z(i-n) \quad (3.11)$$

where $z(i)$ is uncorrelated and Gaussian distributed white noise of zero mean, $z = 0$, and variance $\sigma_z^2 = (1-\lambda^2)\sigma_x^2$. For $\lambda = 0$ one obtains white noise, $0 < \lambda < 1$ defines red noise as a first-order AR-process; for $\lambda = 1$ (3.11) defines a random walk, which is nonstationary, because $\sigma_x^2 = \sigma_z^2 \sum \lambda^{2n} = \sigma_z^2/(1-\lambda^2)$ tends to infinity for $n \to \infty$.

Now the distance between independent pairs of points (embedded in a m-dimensional phase space) can be deduced, considering the single variable SOI to be represented by zero ($\lambda = 0$), first ($0 < \lambda < 1$) or higher order AR-process with time step $\tau = t_i - t_{i-1}$:

$$|x_m(t_i) - x_m(t_j)|^2 = \sum_{\gamma=0}^{m-1} (x(t_i + \gamma\tau) - x(t_j + \gamma\tau))^2$$

$$= \sum_{\gamma=0}^{m-1} [z(i+\gamma\tau) - z(j+\gamma\tau) + \lambda^1(z(i+\gamma\tau - 1) - z(j+\gamma\tau - 1)) + \cdots]^2. \quad (3.12)$$

Since a linear combination $y = az_1 + bz_2$ of Gaussian random variables z_1 and z_2 is Gaussian distributed with mean $y = az_1 + bz_2$ and variance $\sigma_y^2 = a^2\sigma_1^2 + b^2\sigma_2^2$, the sum of the squared distance components (of the normalized variable x) is χ^2-distributed with m degrees of freedom:

$$C_m(\chi) = \text{prob}\{|x_m(t_i) - x_m(t_j)|^2 \leq \chi^2\} = P(\chi^2|m). \quad (3.13)$$

$l^2 = 2\sigma_x^2\chi^2$ when comparing (3.13) with (2.6). The Abramowitz and Stegun (1965, Eq. 26.4.1) notation has been used for the chi-square probability function, $P(\chi^2|m)$. Note that this distribution is unaffected by the (zero or first) order of the AR-process; only the Gaussian distribution of the random variables matters. This is obvious when applying the rules of the linear combination of Gaussian variables to (3.12) and realizing $\sigma_x^2 = \sigma_z^2 \sum \lambda^{2n} = \sigma_z^2/(1-\lambda^2)$ for normalizing the distance components.

The order-2 entropy and pointwise dimension of the Gaussian process can now be deduced as lower bounds for the Kolmogoroff entropy and the information dimension:

$$K_2 = \frac{1}{\tau} \ln \frac{P(\chi^2|m)}{P(\chi^2|m+1)} = \infty,$$

$$D_2 = \frac{d \ln P(\chi^2|m)}{d \ln \chi} = m \quad \text{for} \quad l = \chi \to 0. \quad (3.14)$$

These results can be derived using the l'Hospital rule for both K_2 and D_2 and applying the Leibniz rule only to D_2 with a substitution of $\ln\chi = u$, say. The known fact appears that the dimension of a random process scales with the embedding dimension ($D_2 \sim m$) and that the degree of chaos, K_2, is infinite (or its predictability vanishes $1/K_2 \sim 0$). Note that the finite predictability of the binary El Niño/La Niña time series [(3.8) with $p_0 = p_1 = 0.5$] was due to the number of only two discrete states to be predicted. An increasing number of equally probable states leads to zero predictability [§3a(1)] as it is also obtained by the continuous random process (3.14); i.e. there is no predictability of a random continuous state time series beyond the sampling or averaging time ($\tau = 1$ year) for which the signal is representative. In appendix A the distance distributions obtained from an observed time series of the Southern Oscillation index are compared with a related Gaussian random process.

4. Nonlinear deterministic analysis of El Niño and the Southern Oscillation

A nonlinear deterministic analysis is applied to the two time series of the El Niño/Southern Oscillation process to complement the stochastic analysis. Quinn et al. (1978; updated by Rasmusson 1984) define intensities of annual El Niño events (very weak, weak, strong, very strong) for the year of their onset. Numbers from 0 for no El Niño (or La Niña) to 4 for strong El Niño quantify the intensities and generate a measurable time series on which a distance (2.5) can be defined. Only the 140 years from 1844 to 1983 are used, when

FIG. 1. Distributions of period lengths, recurrence and first passage times based on 140 years (1844–1983) of El Niño/La Niña binary observations (Quinn et al. 1978; updated by Rasmusson 1984): empirical distributions (columns), distributions of the fitted first order Markov chain (×), distributions of the zero order (or climate) Markov chain (O). For details see appendix B.

pressure observations become available to define the strength of the ENSO episodes.

Wright's (1975, personal communication) updated annual Southern Oscillation index covers the year from April to March. It depends on weighted surface pressure observed at eight representative stations (Capetown, Bombay, Djakarta, Darwin, Adelaide, Apia, Honolulu, Santiago). Only the last hundred years (1884–1983) will be used.

These variables (El Niño intensity and Southern Oscillation index) represent two different time series which will be analyzed as outlined in section 2. Note that only one single variable of a dynamical system, which is embedded in a sufficiently high dimensional phase space spanned by time lagged coordinates, allows a description of the basic geometrical properties of the time evolution (occurring on an attractor): the dimensionality of the attractor and the mean rate of divergence of initially close pieces of trajectories evolving on it. Note also that time series that are too short do not allow us to draw conclusions which go beyond estimates of very weak lower bounds to the Kolmogoroff entropy (and dimensionality) of the dynamics of the ENSO process evolving on an attractor, in particular if the attractors of the hydrodyamic flows have dimension > 5 (Swinney and Gollub 1986; see also Grassberger 1986; Nicolis and Nicolis 1987).

The cumulative distance distributions of the Southern Oscillation index trajectory pieces are shown in a $\ln C_m(l)$ versus $\ln l$ plot for embedding dimensions up to $m = 20$ using a delay time of $\tau = 3$ years, (Fig. 2). One observes (also for $\tau = 1$ and 2 years, which are not shown) that for small distances l their slopes tend to increase with increasing embedding dimension (which holds for $\ln l < 3.5$). This indicates the randomness of the time series (as tested in appendix A for small embedding dimensions and for $\tau = 1$ year as an example). The related dimensionality $D_2 \sim m$ of the attractor and the K_2-entropies reveal a small predictability time scale (e.g. at $m = 20$: $D_2 \sim 20$ and $1/K_2 \sim 1$–2 years). Note that for random processes (e.g. white noise) the attractor dimension increases with the embedding dimension $D_2 \sim m$ (§3b). However, there is a distance l-range ($\ln l > 3.5$) where $\ln C_m(l)$ versus $\ln l$ graphs reveal a knee with smaller slopes (dimension) $D_2 \sim 4$–5 and larger predictability time scales $1/K_2 > 15$ years.

As this scaling regime occurs only when the embedding dimension is large ($m > 12$) and disappears when analyzing the time series with a delay time $\tau = 1$ and 2 years, it may well be due to sampling without physical causes. If, however, we accept its reality, such a knee may allow a physical interpretation (e.g., see Eckmann and Ruelle, 1985). The attractor of the observed El Niño/Southern Oscillation process may consist of two subsystems (e.g., the ocean on the one hand and the tropical atmosphere on the other). The subsystem with lower dimensionality and longer predictability (e.g., the ocean or a part of the coupled atmosphere–ocean system) is related to the larger distance scales ($\ln l > 3.5$, in Fig. 2). In the smaller scale domain ($\ln l < 3.5$) the complete atmosphere–ocean system contributes to the observed time series in its dimensionality and predictability. Either the larger-scale subsystem

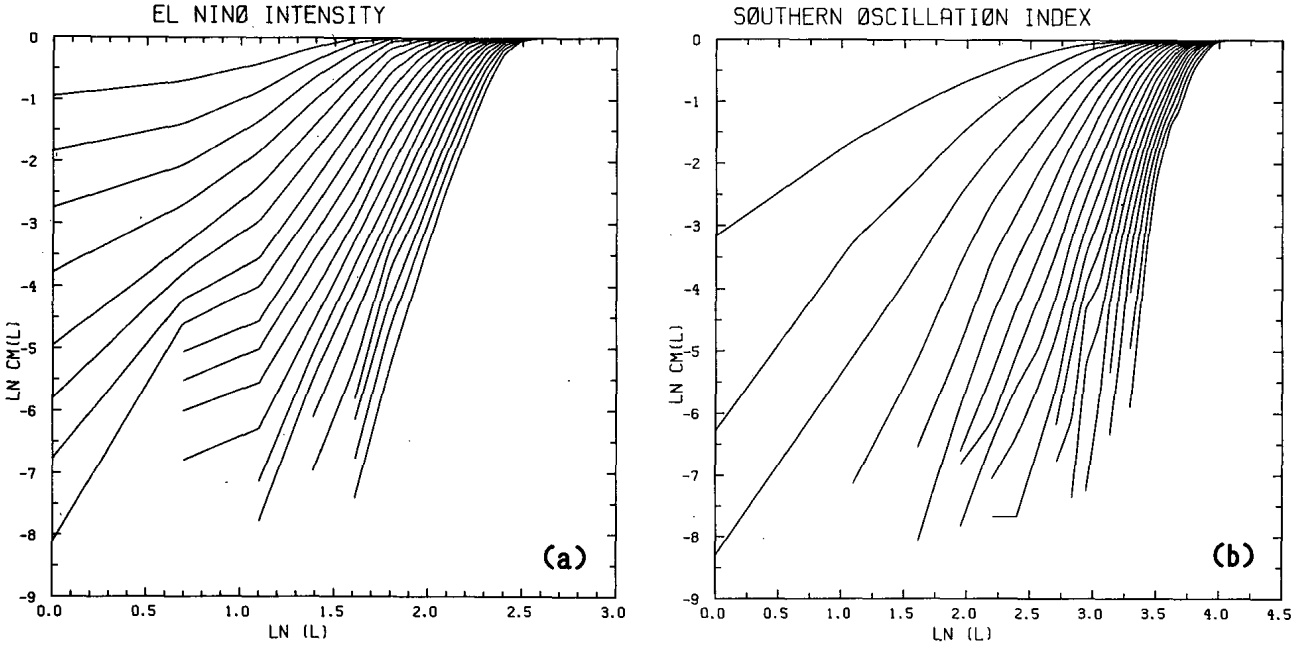

FIG. 2. Cumulative distribution functions $C_m(l)$ displayed in a $\ln C_m(l)$ versus $\ln l$ diagram for a sequence of embedding dimensions ($m = 1$, to 20) increasing from left to right: (a) El Niño intensities (140 years, $\tau = 3$ years, $|t_i - t_j| > 5$ years). (b) Southern Oscillation index (100 years, $\tau = 3$ years, $|t_i - t_j| > 5$ years).

drives the smaller scale, or, which seems to be the case here, noise effects are so large that they dominate all but a small fraction of the attractor. Note that the lower dimensional subsystem ($\ln l > 3.5$) may be characterized by contributions from both parts of the coupled atmosphere and ocean system, as the dimensionality estimates do not give information about physical details but simply lower bounds for the degrees of freedom involved.

On first sight this result may appear to be comparable with dimension estimates from Hense (1987), who claimed a fractal dimensionality between 2.5 and 6 for the Southern Oscillation attractor based on monthly mean precipitation, pressure and sea surface temperature time series. Because the K_2-entropies (estimated from the graphs) reveal predictability time scales of a couple of months only (these are deduced from the same distance domains as the dimensionality), they may have captured only the strong annual cycle of the time evolution (which we wanted to avoid, see Introduction) with ENSO and other signals generating random noise on the smaller distance scales.

The cumulative distance distributions of trajectory pieces taken from El Niño intensities (Quinn et al. 1978) show similar behavior but without indication of a knee. The $C_m(l)$ graphs in the $\ln C_m(l)$ versus $\ln l$ diagram (Fig. 2a) do not tend to a saturation dimension when increasing the embedding with $\tau = 1, 2, 3$ years time lag (for $\tau = 1$ at $m = 20$: $D_2 \sim 11$–12 and $1/K_2 \sim 1.5$ to 2.5 years of e-folding error growth; for $\tau = 3$ years: $D_2 \sim 11$–12 at $m = 20$, but $1/K_2 \sim 5$ years which reduces with increasing m and decreasing l). Note that due to the short length of the time series, these dimension and K_2-entropy estimates provide only very weak lower bounds.

5. Conclusion

In summation, the results from annual ENSO time series analyses do not yet provide a clear support of the ideas that there is a (strange) ENSO attractor of low dimensionality on which the time evolution shows error doubling time scales of more than one year. On the contrary, the time series analyses tend to support stochastic and/or higher dimensional effects on the time evolution of the coupled atmosphere–ocean large-scale dynamics. Accordingly, predictability time scales show error doubling times of the order of the sampling time. Because the time series available are only of short lengths, these conclusions may not be regarded as final, in particular, when considering the limitations experienced in analyzing hydrodynamic flow with attractors whose fractal dimensionality > 5 (Swinney and Gollub 1986); i.e. the number of independent but similar (or analogue) infinitesimally close pieces of trajectories appears to be too small to estimate (quantify) features of chaotic behavior: dimensionality and predictability (or the degree of chaos).

These results seem to be supported by present day numerical modeling (Cane et al., 1986) claiming predictability of ENSO of about one to two years. Given realistic initial conditions many features of an ENSO event appear to be predictable within this time span. However, predicting longer lead times, e.g., into the following episode, let it be a La Niña or El Niño event, seems to be difficult; at least this analysis (based on the presently available datasets) suggests that predictions would double their initially (infinitesimally small) errors in a year. Physically, this seems to make sense because there is an annual "peak" of instability (in April) when the coupled ocean–atmosphere system is most unstable. However, as Philander and Lau (1986) suggest, it may be "possible for the occurrence of El Niño at a given time to depend . . . on the occurrence of an earlier El Niño." A very weak indication of this appears in the analysis of the annual Southern Oscillation index (Fig. 2, but only when embedding it into a phase space of multiples of $\tau = 3$ years time lagged coordinates). For building prediction schemes this leads to the conclusion that predictions are possible for at least one to two years ahead (i.e. with initially small errors doubling within this time scale) which allow basically *nowcasting* the El Niño/Southern Oscillation phenomenon.

Acknowledgments. Thanks are due to Ms. C. Aiello and Fay Stroumos for typing, M. Manton and N. Nicholls for reading the manuscript, Peter Webster and Michael Ghil for their constructive reviews which helped improve the paper.

APPENDIX A

Test for the Grassberger-Procaccia Algorithm Applied to Binary and Continuous State Time Series

1. Binary states

The following hypothesis suggested in section 3 needs to be tested. The El Niño intensity time series (based on Quinn et al. 1978, updated by Rasmusson 1984) with La Niña ($x(t) = 0$) and El Niño ($x(t) = 1$) events and a Bernoulli experiment of almost unbiased coinflips produce similar distance distributions between pairs of points (or pieces of trajectories in time lagged phase space). The cumulative distribution of the empirical time series is calculated from (2.7) and (3.2) with $\tau = 3$ years and $|t_i - t_j| > 5$ years. The cumulative distribution of the random (biased) coinflip time series is defined by (3.6) using (3.4).

For embedding dimensions $m = 1, 2, 3$ the probabilities (not the cumulative distribution) are shown in Table 2a, to which a chi-square goodness of fit test can be applied. With the total number of observed distance values $N^2 = (140 - 5 - 3m)(140 - 5 - 3m - 1)/2$ one obtains chi-square $= \sum N^2(\text{ENSO} - \text{RANDOM})^2/\text{RANDOM}$ with m degrees of freedom. From first sight

TABLE 2. Estimated and theoretical probabilities of distance, l, between pairs of points (or pieces of trajectories embedded into m-dimensional phase space) of (a) 140 years binary El Niño/Southern Oscillation time series (ENSO) and a random or biased coinflip (RANDOM), (b) 100 years continuous state Southern Oscillation index (SOI) and a Gaussian stochastic process (Gauss).

		Embedding dimension					
		$m = 1$		$m = 2$		$m = 3$	
		(a) Binary states					
Distance		Random	ENSO	Random	ENSO	Random	ENSO
$l^2 = 0$		.5162	.5126	.2664	.2650	.1376	.1345
$l^2 = 1$		.4838	.4874	.4996	.5028	.3867	.3893
$l^2 = 2$				.2340	.2322	.3625	.3629
$l^2 = 3$						.1132	.1133
N^2		8646		8256		7875	
Chi-square		0.4487		0.3988		0.6918	
		(b) Continuous states					
l^2	χ^2	Gauss	SOI	Gauss	SOI	Gauss	SOI
≤1	≤.01	.0806	.0421	.0051	.0025	.0002	.0002
1–3	.01–.03	.1504	.1548	.0401	.0399	.0071	.0062
3–5	.03–.05	.1549	.1522	.0753	.0698	.0252	.0297
5–7	.05–.07	.1364	.1432	.1024	.1041	.0496	.0486
7–9	.07–.09	.1162	.1130	.1179	.1120	.0766	.0729
>9	>.09	.3615	.3947	.6592	.6717	.8413	.8424
N^2		4371		4278		4186	
Chi-square		87.56		7.73		4.68	

the similarity between the ENSO and random or biased coinflip probabilities seems to be obvious, which is confirmed on a 5% significance level.

2. Continuous states

The following hypothesis needs to be tested which is related to the continuous time series of a Southern Oscillation index (SOI, based on Wright 1975 and updated). The observed SOI and a Gaussian stochastic process of the same variance, σ_x^2, produce similar distance distributions between pairs of points (or pieces of trajectories in the time lagged phase space). The cumulative distribution of the empirical time series $C_m(l)$ is calculated from (2.5) and (3.2) with $\tau = 1$ year and $|t_i - t_j| > 5$ years. The cumulative distribution of the Gaussian process is defined by (3.13). The normalization, $\chi^2 = l^2/2\sigma_x^2$, by the variance of the distance components, $2\sigma_x^2 = 97.13 \sim 100$, relates the empirical $C_m(l)$ to the chi-square (cumulative) distance distribution $P(\chi^2 | m)$ of the Gaussian process, which is obtained from Abramowitz and Stegun (1965, Table 26.7) and shown in Fig. 3. In Table 2b the probabilities of classes of small distances are given in detail. Now a chi-square goodness of fit test is applied to the first $k = 2, 3, 5$ (for $m = 1, 2, 3$ embedding dimensions) classes of small distances when $C_m(l)$ or $P(\chi^2 | m) < 15\%$ (to account for the limit process $l \to 0$ in predictability and dimensionality analysis) plus one further class to cover the remaining distance values. With the total number of observed distance values $N^2 = (100 - 5 - m)(100 - 5 - m - 1)/2$ one obtains chi-square $= \sum N^2 (\text{GAUSS} - \text{SOI})^2/\text{GAUSS}$ for $k + 1$ terms; i.e. with k degrees of freedom, as the σ_x^2-estimate has been used for normalizing the theoretical distance distribution $P(\chi^2 | m)$. On a 5% significance level the similarity between the empirical SOI and a Gaussian process is confirmed for embedding dimensions $m = 2$ and 3, but not for $m = 1$. This is not surprising because only integer SOI-values enter the time series which, in particular for low embedding dimensions, effects the assumption of a continuous state variable.

APPENDIX B

Time Distributions

The *residence time* $L_k = n$ is the time for which the process stays in one and the same state $x(t) = k$ before leaving for another. Its distribution is formally defined

$$P(L_k = n) = \text{prob}\{x(t + (n + 1)\tau) \neq k | x(t + n\tau) = x(t + (n - 1)\tau) = \ldots = x(t) = k\}.$$

For Markov chains one obtains a geometric distribution for the residence time of state k:

$$P(L_k = n) = p_{kk}^{n-1}(1 - p_{kk})$$

with mean $(1 - p_{kk})^{-1}$ and variance $p_{kk}(1 - p_{kk})^{-2}$.

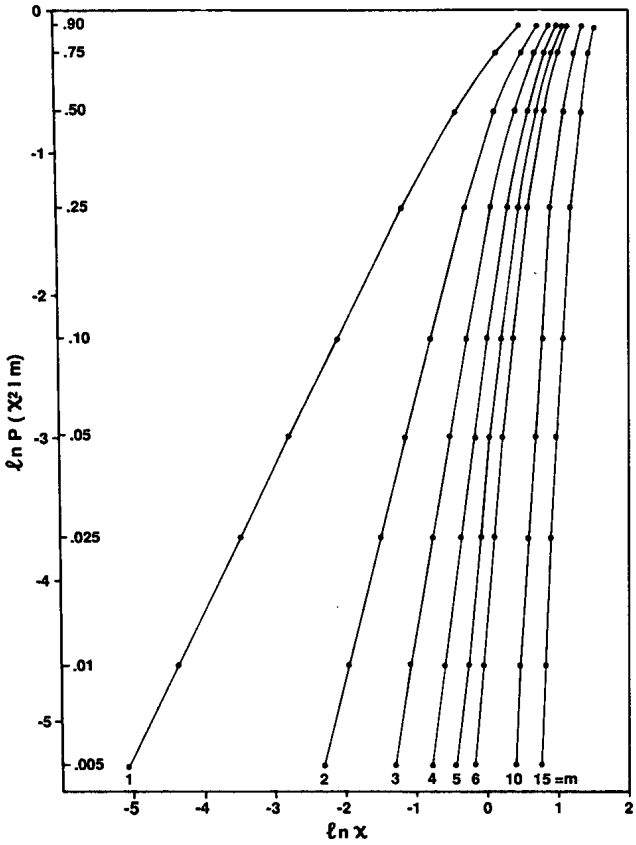

FIG. 3. Cumulative distribution functions $P(\chi^2|m)$ displayed in a $\ln P(\chi^2|m)$ versus $\ln\chi$ diagram for a sequence of embedding dimensions (m = 1, 2, 3, 4, 5, 6, 10, 15) increasing from left to right (see section 3b and appendix A for more details).

Thus residence times of the zero-order Markov chain are defined by the climate probabilities p_k entering $P(L_k = n)$.

The *first passage time* $T_{kl} = m$ elapses between state k and the first visit to state l, which has been avoided at times $t \leqslant t + \nu\tau \leqslant t + (m-1)\tau$:

$$P(T_{kl} = m) = f_{kl}^{(m)} = \text{prob}\{x(t + m\tau) = l | x(t + \nu\tau) \neq l \text{ for } 1 \leqslant \nu \leqslant m-1;\ x(t) = k\}.$$

The *recurrences time* $T_{kk} = m$ elapses between state k and the first visit to the same state k but avoiding it at times in between $t \leqslant t + \nu\tau \leqslant t + (m-1)\tau$. The first passage probability for Markov chains can be evaluated successively from the transition probabilities:

$$p_{kl}^{(m)} = \sum_{r=0}^{m} f_{kl}^{(r)} p_{ll}^{(m-r)}$$

with $f_{kl}^{(0)} = 0$ and $p_{kl}^{(0)} = 1$. Mean and variance can also be deduced in matrix form (e.g. Kemeny and Snell 1976).

One special case is the return probability $f_{kk}^{(m)}$ for which the mean recurrence time $\langle T_{kk} \rangle = p_k^{-1}$ is given by the inverse of the climate state probability; i.e. it is identical with the mean residence time of all the remaining states with probability $(1 - p_k)$.

Another special case arises, when the transition matrix is represented by the climate (or zero order) Markov chain. For this case one can derive $f_{kl}^{(m)} = p_{ll}(1 - p_{ll})^{m-1}$; i.e. the distribution of the residence time of El Niño to La Niña is identical with the distribution of the recurrence time from La Niña to La Niña (El Niño to El Niño) and the first passage time from El Niño to La Niña (La Niña to El Niño).

REFERENCES

Abramowitz, M. and J. A. Stegun, 1965: Handbook of *Mathematical Functions.* U.S. Govt. Printing Office, 1046 pp.

Anderson, T. W., and L. A. Goodman, 1957: Statistical inference about Markov chains. *Ann. Math. Stat.*, **28,** 89–109.

Barnett, T. P., 1984: Prediction of the El Niño of 1982–83. *Mon. Wea. Rev.*, **112,** 1403–1407.

Cane, M. A., S. E. Zebiak and S. C. Dolan, 1986: Experimental forecasts of El Niño. *Nature,* **321,** 827–832.

Cox, D. R., and H. D. Miller, 1965: *The Theory of Stochastic Processes.* Champman and Hall, 398 pp.

De Swart, H. E., and J. Grasman, 1987: Effect of stochastic perturbations on a low-order spectral model of the atmospheric circulation. *Tellus,* **39A,** 10–24.

Eckmann, J. P., and D. Ruelle, 1985: Ergodic theory of chaos and strange attractors. *Rev. Mod. Phys.*, **57,** 617–656.

Farmer, J. D., 1982: Information dimension and probabilistic structure of chaos. *Z. Naturforsch.*, **37a,** 1304–1325.

Feller, W., 1950: *An Introduction to Probability Theory and Its Applications,* Vol. I, Wiley and Sons, 509 pp.

Fraedrich, K., 1986: Estimating the dimensions of weather and climate attractors. *J. Atmos. Sci.*, **45,** 419–432.

——, 1987a: Estimating weather and climate predictability on attractors. *J. Atmos. Sci.*, **46,** 722–728.

——, 1987b: El Niño iterations. *Beitr. Phys. Atmos.* **60,** 22–33.

Ghil, M., and S. Childress, 1987: *Topics in Geophysical Fluid Dynamics: Atmospheric Dynamics, Dynamo Theory, and Climate Dynamics.* Springer-Verlag, 1–485.

Grassberger, P., 1986: Do climatic attractors exist? *Nature,* **232,** 609–612.

——, and I. Procaccia, 1983: Estimation of the Kolmogoroff entropy from a chaotic signal. *Phys. Rev.*, **A23,** 2591–2593.

——, and ——, 1984: Dimensions and entropies of strange attractors from a fluctuating dynamics approach. *Physica,* **13D,** 34–54.

Hense, A., 1987: On the possible existence of a strange attractor for the Southern Oscillation. *Beitr. Phys. Atmos.*, **60,** 34–47.

Kemeny, F. G., and F. L Snell, 1976: *Finite Markov Chains.* Springer-Verlag, 210 pp.

Lorenz, E. N., 1965: A study of the predictability of a 28-variable atmospheric model. *Tellus,* **27,** 321–333.

Lorenz, E. N., 1984: Some aspects of atmospheric predictability. *Problems and Prospects in Longer and Medium Range Weather Forecasting.* D. M. Burridge and E. Kallen, Eds., Springer-Verlag, 1–20.

——, 1985: The growth of errors in prediction. *Turbulence and Predictability in Geophysical Fluid Dynamics and Climate Dynamics,* M. Ghil, R. Benzi and G. Parisi, Eds., North Holland, 243–265.

Lowry, P. W., and D. Guthrie, 1968: Markov chains of order greater than one. *Mon. Wea. Rev.*, **96,** 798–801.

Nicolis, C., and G. Nicolis, 1984: Is there a climatic attractor? *Nature,* **311,** 529–532.

——, and ——, 1987: Evidence for climatic attractors. *Nature,* **326,** 523.

Mo, K. C., and M. Ghil, 1987: Statistics and dynamics of persistent anomalies. *J. Atmos. Sci.*, **44,** 877–901.

Packard, N. J., J. P. Crutchfield, J. D. Farmer and R. S. Shaw, 1980: Geometry from a time series. *Phys. Rev. Lett.*, **45,** 712–716.

Pesin, Ya. B., 1977: Lyapunov characteristic exponents and smooth ergodic theory. *Russian Math. Survey,* **32(4),** 55–114.

Philander, S. G. H., 1985: El Niño and La Niña. *J. Atmos. Sci.*, **42,** 2652–2662.

——, and N.-C. Lau, 1986: Predictability of El Niño. *Physically Based Modelling and Simulation of Climate and Climate Change.* M. Schlesinger, Ed., NATO Advanced Study Institute Series. D. Reidel.

Quinn, W. J., D. O. Zopf, K. S. Short and R. T. W. Kuo Yang, 1978: Historical trends and statistics of the Southern Oscillation, El Niño, and Indonesian droughts. *Fish. Bull.* **76,** 663–678.

Rasmusson, E. M., 1984: El Niño: The ocean/atmosphere connection. *Oceanus,* **27,** 5–12.

Swinney, H. L., and J. P. Gollub, 1986: Characterization of hydrodynamic strange attractors. *Physics,* **18D,** 448–454.

Takens, F., 1981: Detecting strange attractors in turbulence. *Dynamical Systems and Turbulence,* Warwick, 366–381.

Vallis, G. K., 1986: El Niño: A chaotic dynamical systems? *Science,* **232,** 243–245.

Wright, P. B., 1975: An index of the Southern Oscillation. Climatic Research Unit, University of East Anglia, Norwich, 22 pp.

——, 1984: Relationships between indices of the Southern Oscillation. *Mon. Wea. Rev.*, **112,** 1913–1919.

——, 1985: The Southern Oscillation: An ocean–atmosphere feedback system? *Bull. Amer. Meteor. Soc.*, **66,** 398–412.